JACS
JOURNAL OF THE AMERICAN CHEMICAL SOCIETY
Article
pubs.acs.org/JACS

The Mechanism of Iron(II)-Catalyzed Asymmetric Mukaiyama Aldol Reaction in Aqueous Media: Density Functional Theory and Artificial Force-Induced Reaction Study

W. M. C. Sameera,[†] Miho Hatanaka,[†] Taku Kitanosono,[‡] Shū Kobayashi,[‡] and Keiji Morokuma*[,†]

[†]Fukui Institute for Fundamental Chemistry, Kyoto University, Kyoto 606-8103, Japan
[‡]Department of Chemistry, School of Science, The University of Tokyo, Hongo, Bunkyo-ku, Tokyo 113-0033, Japan

Supporting Information

ABSTRACT: Density functional theory (DFT), combined with the artificial force-induced reaction (AFIR) method, is used to establish the mechanism of the aqueous Mukaiyama aldol reactions catalyzed by a chiral Fe(II) complex. On the bases of the calculations, we identified several thermodynamically stable six- or seven-coordinate complexes in the solution, where the high-spin quintet state is the ground state. Among them, the active intermediates for the selectivity-determining outer-sphere carbon−carbon bond formation are proposed. The multicomponent artificial force-induced reaction (MC-AFIR) method found key transition states for the carbon−carbon bond formation, and explained the enantioselectivity and diastereoselectivity. The overall mechanism consists of the coordination of the aldehyde, carbon−carbon bond formation, the rate-determining proton transfer from water to aldehyde, and dissociation of trimethylsilyl group. The calculated full catalytic cycle is consistent with the experiments. This study provides important mechanistic insights for the transition metal catalyzed Mukaiyama aldol reaction in aqueous media.

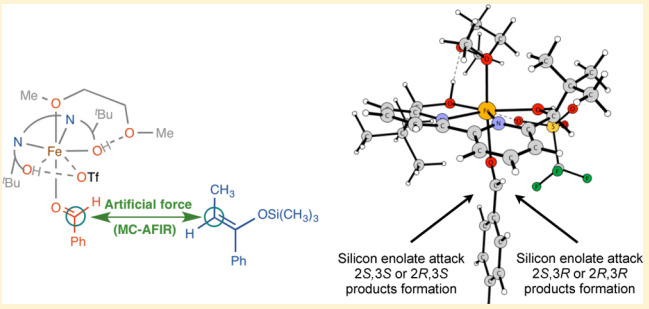

INTRODUCTION

Transition metal homogeneous catalysis is one of the most efficient ways to perform carbon−carbon bond formation reactions in a controlled and a selective fashion. The Suzuki−Miyaura reaction,[1,2] Heck-type reactions,[3−6] Wittig reaction and its many variants,[7,8] olefin metathesis,[9−13] cross-coupling of diazo compounds[14−18] are popular carbon−carbon bond formation reactions. These synthetic reactions have become indispensable for extensive applications in both industry and academia. Development of versatile synthetic procedures that lead to efficient and highly selective carbon−carbon bond formation under mild conditions is still an active area of research.

The aldol reaction is a fundamental and reliable method for carbon−carbon bond formation.[19−22] The classical aldol reactions work under heating Brønsted acidic or basic conditions. The yields depend on the substrates because of the reversibility of the reaction. Many competitive reactions, such as self-condensation, dehydration, and polymerization, are also major challenges in this area. Most of these side reactions can be avoided by using the Lewis acid catalyzed cross-aldol reactions of silicon enol ethers or ketene silyl acetal as nucleophiles, the so-called Mukaiyama aldol reaction.[23−25] Lewis acids, such as $TiCl_4$, can be used as the catalysts in this reaction, and highly enantioselective transformations can be achieved by using the chiral Lewis acid catalysts.[20,26−28]

Typically, Lewis acids are inactive under the hydrous condition. The Kobayashi modification to the Mukaiyam aldol reaction, however, utilizes Lewis acids under hydrous condition.[29−32] For instance, rare earth trications and several dicationic transition metals, such as Fe, Cu, Zn, Cd, and Pd, are active catalysts in aqueous media.[33] Asymmetric versions of the Mukaiyama aldol reactions have also been achieved in aqueous media using chiral catalysts.[34−43] One of the successful catalytic systems is Fe(II) with the Bolm's ligand[44] (L1) as shown in Scheme 1.[45,46] Relatively high enantioselectivity is achieved for a number of aromatic and nonaromatic aldehydes by using the

Scheme 1. Aqueous Mukaiyama Aldol Reaction of Silyl Enol Ethers with Aldehydes Catalyzed by Fe(II) with Bolm's Ligand (L1)

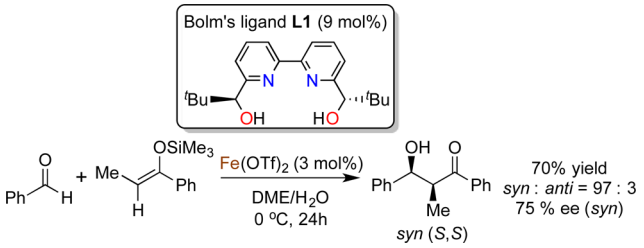

Received: June 5, 2015
Published: August 12, 2015

DOI: 10.1021/jacs.5b05835
J. Am. Chem. Soc. 2015, 137, 11085−11094

Fe(II) catalyst. The ligand L1 has been used for aqueous asymmetric reactions, such as hydromethylation reactions,[47−50] ring-opening reactions,[51,52] and Nazarov cyclizations.[53] The X-ray structures of Fe(II),[45] Sc(III),[47] and Bi(III)[48] with the ligand L1 were characterized, and they have the pentagonal bipyramidal structures. The X-ray structure of Fe(II) complex incorporates a water molecule and a DME molecule.[45] Kitanosono et al. have studied the ESI-MS spectra[46] under the reaction conditions, and several Fe(II) complexes, such as $[(L1)Fe(OTf)]^+$ and $[(L1)Fe(DME)(OTf)]^+$, were observed. The catalytic ability of Fe(II) and Fe(III) was also compared; the reaction with Fe(III) gives rise to very low yield (15%) and poor enantioselectivity (1% ee).[34] The diastereoselectivity of the reaction is however independent of the oxidation state of Fe.[34] Ollevier et al. also reported a similar trend for the Mukaiyama aldol reaction catalyzed by Fe(III) perchlorate system (25% yield and 52% ee).[45]

The mechanism of Mukaiyama aldol reaction is a matter of controversy. Two mechanistic proposals can be found in the literature. Moreover, the Mukaiyama aldol reaction catalyzed by lanthanide in aqueous media proceeds through a stepwise mechanism. The first step is the carbon−carbon bond formation. Followed by proton transfer from water to aldehyde, and finally by dissociation of trimethylsilyl dissociates via a nucleophilic attack of water molecules.[70] However, a concerted mechanism is proposed for the Mukaiyama Aldol reaction without Lewis acid catalyst.[54,55]

In developing quantitative mechanistic understanding of the Mukaiyama aldol reactions, computational studies become critical. Although many theoretical studies of aldol reactions have been reported in the literature,[55−66] only few studies are focused on the Lewis-acid catalyzed Mukaiyama aldol reactions. Wong and co-workers[67,68] used simplified model systems to study the metal chloride-promoted Mukaiyama aldol reactions of trihydrosilyl enol ethers with formaldehyde. According to their density functional theory (DFT) and Møller−Plesset (MP) perturbation theory studies, the reaction occurs through a concerted carbon−carbon bond formation and chloride transfer to the trihydrosilyl enol ether, which is the rate-determining step. The same group studied a similar reaction promoted by diatomic halogens as the Lewis acids, and this reaction also occurs through a concerted carbon−carbon bond formation and trihydrosilyl transfer. However, a stepwise mechanism was suggested for the halogen-catalyzed reaction of benzaldehyde with the trimethylsilyl (TMS) protected silyl enol ether of acetophenone, while the carbon−carbon bond formation is the rate-determining step. Helquist and Wiest reported a DFT study on the diastereoselectivity of Lewis-acid catalyzed Mukaiyama aldol reactions (without water condition).[69] By analyzing the conformations of the transition states of seven different pathways, they concluded that the pro-*anti* pathways occur through "antiperiplanar" transition structures, while the pro-*syn* pathways favor "synclinal" transition structures.

Systematic sampling of transition states that lead to carbon−carbon bond formation is challenging, and is critical in terms of calculating the diastereomeric ratio or enatiomeric excess of the reaction. Toward the conformation sampling, the artificial force-induced reaction (AFIR) method[70,71] in the Global Reaction Route Mapping (GRRM) strategy[72] is very useful. This is an effective way to search many important reaction pathways, namely local minima (LMs) and transition states (TSs). This method was used for the study of the Eu catalyzed Mukaiyama aldol reaction in water.[73,74] Further, more than 160 TS structures were found for the selectivity determining carbon−carbon bond formation step, and about 10 of them contributed to the diastereoselectivity of the reaction.

In this study, we performed DFT calculations combined with the AFIR search method to establish the mechanism of the full catalytic cycle, and the diastereoselectivity, and enantioselectivity of Fe(II)-calalyzed aqueous asymmetric Mukaiyama aldol reaction (Scheme 1). A particular emphasis is the diastereo and enantioselectivity determining carbon−carbon bond formation step, in which a large number of transition state conformations need to be sampled to clarify the origin of the selectivity. This was realized by the use of the automatic search AFIR method.[70−72] A full mechanism of the catalytic cycle is established.

COMPUTATIONAL METHODS

Unless otherwise stated, all structure optimizations were carried out using B3LYP-D3[75−78] functional as implemented in the Gaussian09 program.[79] The SMD model was used as the implicit solvent model with the direct constant of ε = 78.3553 (water).[80] The SDD basis set and associate effective core potential was applied for iron,[81,82] 6-31+G(d) basis set for oxygen and nitrogen, and 6-31G(d) basis set for the other atoms (BS1).[83−86] All structures were fully optimized without restrictions. Vibrational frequency calculations were performed to establish the nature of the stationary points (LMs or TSs). Pseudo-IRC calculations (a few steps of IRC followed by optimization) confirmed the connectivity between TSs and LMs. Single-point energies of the optimized structures were recalculated with the SDD basis set for iron and cc-pVTZ basis set for other atoms (BS2).[87−89]

In the Results and Discussion section, we report ΔG (the Gibbs free energy) at 273.15 K and 1 atm, and ΔE (the electronic energy) with the zero point energy correction. There are different arguments concerning the quenching of entropy contributions in solution. Some authors suggested scaling, while others suggested truncation. The reality seems to lie between the two extremes.[90−96] When the number of molecules changes during the reaction, it is important pay attention to the difference between the Gibbs free energy and the electronic energy with ZPE. For diastereoselectivity or enantioselectivity, we compare TS conformations with the same number of molecules, and the entropy difference comes essentially from the tightness of the TSs.

Many conformations with nearly same energy may exist for the TSs of the carbon−carbon bond formation step, and need to be properly sampled. This was achieved by the AFIR search,[70−72] as implemented in the GRRM program.[97] Since the system is very large, we have used ONIOM(B3LYP-D3:PM6-D3) method to obtain the energy and derivatives.[98−103] The partitioning of the molecular system is shown in Scheme 2a. The LanL2DZ basis sets and associated effective core potentials were applied for the all atoms (BS3) in the high-level region[82,104−106] The SMD model was used as the implicit solvent

Scheme 2. (a) Partitioning the Molecular System into ONIOM High- and Low-Levels; (b) AFIR Artificial Force Was Applied Only between Fragment 1 (C Atom of the Aldehyde) and Fragment 2 (β-Carbon of Sily Enol Ether)

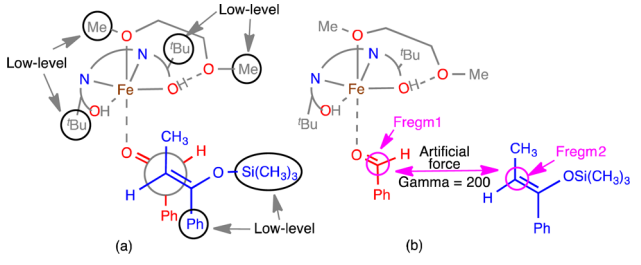

DOI: 10.1021/jacs.5b05835
J. Am. Chem. Soc. 2015, 137, 11085−11094

model with water as the solvent. In the multicomponent AFIR (MC-AFIR), 50 randomly oriented structures were prepared and an AFIR path was determined from each random structure with addition of artificial force between reactive two carbon atoms as shown in Scheme 2b. The artificial force parameter (γ) of 200 kJ mol^{-1} was used, and this was appropriate for finding TSs roughly within this energy. The AFIR search was terminated when no new AFIR LM was found for N_{max} consecutive AFIR paths. Here different conformations of LMs are of course considered to be new and different. In this study, N_{max} = 10 was used. Although not exhaustive nor guaranteed because of the nature of the method. Past experiences suggest that essential pathways are not likely to be missed using this value of N_{max}. The obtained pathways are always inspected manually for obvious omission. At the highest energy points on the AFIR paths (approximate transition states), single-point energies were calculated with B3LYP-D3/BS1. Then, all structures within 20 kcal mol^{-1} from the lowest were fully optimized at the same level without the artificial force. All the fully optimized transition states were used to calculate the ratios of different reaction paths and enantiomeric excess based on the Boltzmann distribution of transition state at 273.15 K and 1 atm.

Energy decomposition analysis (EDA)[107,108] was performed for the lowest energy transition states leading to the (2*S*,3*S*) and (2*R*,3*R*) forms of the product formation step. B3LYP-D3/BS2 level, including SMD solvation effects, was used in this analysis. The B3LYP-D3/BS1 optimized transition states were divided into the catalyst (A), aldehyde (B), and silyl enol ether (C) as shown in Scheme 3. The deformation

Scheme 3. EDA between Two Optimized Transition States for the (2*S*,3*S*) and (2*R*,3*R*) Forms of the Product Formation Step

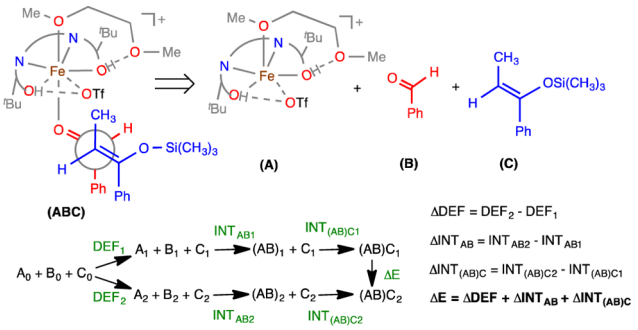

energy (DEF) is the sum of the deformation energy of A, DEF_A (defined as the energy of A at the optimized TS structure relative to that of the optimized isolated structure A_0) and those of B (DEF_B) and C (DEF_C). The first interaction energy term, INT_{AB}, is the interaction energy between A and B at their respective optimized TS structures, while $INT_{(AB)C}$ is the interaction energy between (AB) and C. Using INT_{AB}, $INT_{(AB)C}$, and DEF, energy difference (ΔE) between the two optimized transition states, $(AB)C_1$ and $(AB)C_2$, can be written as a sum of the deformation energy difference (ΔDEF) and interaction energy difference ($\Delta INT_{AB} + \Delta INT_{(AB)C}$).

RESULTS AND DISCUSSION

1. Electronic Structure of Seven-Coordinate [(L1)Fe(II)(DME)(H_2O)]$^{2+}$ Complex (1). Our starting point is a discussion on the electronic structure of seven-coordinate [(L1)Fe(II)(DME)(H_2O)]$^{2+}$ (L1 = Bolm's ligand) complex (**1**). X-ray structure of **1** was reported by Ollevier et al.[45] For a formally d^6 Fe(II) complex in an approximately pentagonal bipyramid environment, three spin states, a singlet, a triplet, and a quintet, are possible. Figure 1 (top) shows the general electronic structure pattern, based on the scheme of Hoffmann and co-workers.[109] In the singlet state, the low-lying d_{xz} and d_{yz} orbitals and one of two metal−ligand σ-antibonding combinations, i.e., d_{xy} or $d_{x^2-y^2}$, are fully occupied. In the triplet state, the metal−ligand σ-antibonding orbitals are singly occupied. Starting from the triplet state, the high-spin quintet state can be formed by transferring a spin-β electron from one of the two low-lying d_{xz} and d_{yz} orbitals to the d_{z^2} orbital.

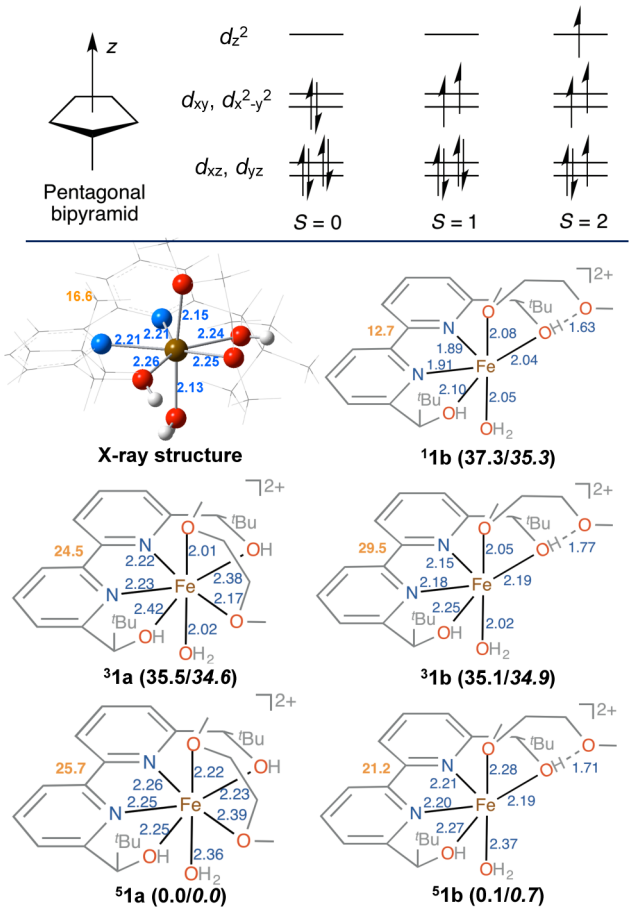

Figure 1. Top: Possible spin states of [(L1)Fe(II)(DME)(H_2O)]$^{2+}$ complex (**1**). Bottom: X-ray structure, and the key structural parameters of the optimized singlet, triplet and quintet states of six- and seven-coordinate complexes of **1**. Relative energies are in kcal mol^{-1} (ΔG values are in plane text, ΔE values are in italics), bond lengths (blue) are in Å and torsion angle (orange) between the two pyridine units of L1 is in degrees.

Optimized structures of various spin states of [(L1)Fe(II)(DME)(H_2O)]$^{2+}$ complex (**1**) and relative energies (ΔG and ΔE) are shown in Figure 1 (bottom), and their net spin densities and $\langle S^2 \rangle$ values are summarized in Table S1 (Supporting Information). The quintet state is thermodynamically most stable, where two structural forms of nearly equal energy are found. One is a seven-coordinate structure (^{5}**1a**), where the calculated $\langle S^2 \rangle$ value of 6.01 and the net spin density on the metal of 3.86 are typical for high-spin Fe(II). The corresponding six-coordinate structure, ^{5}**1b**, is only 0.1/0.7 kcal mol^{-1} higher in free energy G and potential energy (with ZPC) E. Qualitatively similar picture can be observed with the M06L functional, where the energy difference between ^{5}**1a** and ^{5}**1b** become 1.2 and 1.4 kcal mol^{-1} in free energy and potential energy (with ZPC), respectively. The key structural parameters of ^{5}**1a** are in agreement with the X-ray structure. One might speculate that in the crystal, the more compact ^{5}**1a** is more favorable than ^{5}**1b** because of better packing. In solution, both ^{5}**1a** and ^{5}**1b** may be in equilibrium. In the six-coordinate ^{5}**1b**,

DOI: 10.1021/jacs.5b05835
J. Am. Chem. Soc. 2015, 137, 11085−11094

some ligands may coordinate at the vacant site. The triplet state of seven-coordinate (^{3}**1a**) and six-coordinate (^{3}**1b**) complexes are 35.5 and 35.1 kcal mol^{-1} above the ground state (^{5}**1a**), respectively. In both triplet states, calculated $\langle S^2 \rangle$ values, 1.96 of ^{3}**1a** and 1.94 of ^{3}**1b**, are typical for the triplet state. The singlet state, ^{1}**1b**, a six-coordinate structure, lies 37.3 kcal mol^{-1} above the ground state. All attempts for seven-coordinate structure converged to the six-coordinate form; the seven-coordinate singlet structure does not exist. In the presence of fully occupied d_{xy} or $d_{x^2-y^2}$ orbitals with strong metal−ligand σ-antibonding characters, the singlet state leads dissociation of one of the two DME oxygen ligands.

In order to check whether the Hartree−Fock (HF) exchange in the hybrid B3LYP-D3 (20% HF exchange) play a role on the electronic structure, we have repeated our electronic structure analysis with the meta-GGA M06L (0% HF exchange) functional. According to M06L optimized results, the seven-coordinate complex, ^{5}**1a**, is the ground state. Most subtly, in the absence of HF exchanges, energy separations between the three states, total spin density (ρ) of Fe, and $\langle S^2 \rangle$ values are qualitatively similar (Table S1, Supporting Information). Therefore, the HF exchange of the density functional does not play a major role on the electronic structure and relative energy of the possible spin states of **1**.

On the basis of our analysis with the B3LYP-D3 and M06L functionals, we conclude that the thermodynamically stable electronic state of [(L1)Fe(II) (DME)(H$_2$O)]$^{2+}$complex (**1**) is the quintet state, while the triplet or singlet states are significantly higher in energy, suggesting the single-state reactivity (SSR) of this family of complexes. Similar conclusions can be made (Table S2) for three complexes that are relevant to the full catalytic cycle, [(L1)Fe(II) (DME)(H$_2$O) (OTf)]$^+$ (**2**) [(L1)Fe(II) (DME) (OTf)]$^+$ (**4**) and [(L1)Fe(II) (DME) (PhC(O)H) (OTf)]$^+$ (**5**). Therefore, we continue our discussion with the quintet state.

2. Stable and Reactive Prereaction Complexes in Solution. Next we discuss the ligand exchange equilibrium at the Fe(II) center (prior to the carbon−carbon bond formation), and identify thermodynamically stable complexes and reactive complexes for the carbon−carbon bond formation in prereaction solution. In the presence of five potential ligands in the solution, specifically DME, H$_2$O, OTf$^-$, benzaldehyde, and silyl enol ether (denoted as Subs), we would expect an equilibrium among several Fe(II) complexes. It is important to note that concentration of the tetradentate Bolm's ligand (L1) is significantly higher than other ligands in solution. Therefore, in all the complexes we have included this ligand that fills four coordination sites of Fe(II) ion. The remaining three coordination sites (two axial and one equatorial) can be filled by the other ligands in the solution.

Figure 2 summarizes the calculated low-energy structures below 9.5 kcal mol^{-1} in G. All calculated structures are shown in Figure S1. On the basis of the total energy (G) of the complexes, we can find the thermodynamically most stable complexes in solution. Some general rules were found that govern the order of stability. (i) Most of stable complexes (except **4** and **8**) are seven-coordinate systems, suggesting formation of seven-coordinate complexes is favorable. (ii) One DME and one OTf$^-$ ligands are found in the most stable complexes (**2**−**6**), and these two ligands fill two vacant coordination sites at the metal coordination sphere. In these complexes, hydrogen bonding between oxygen atom of OTf$^-$ and −OH unit of L1 is observed, which is important for their

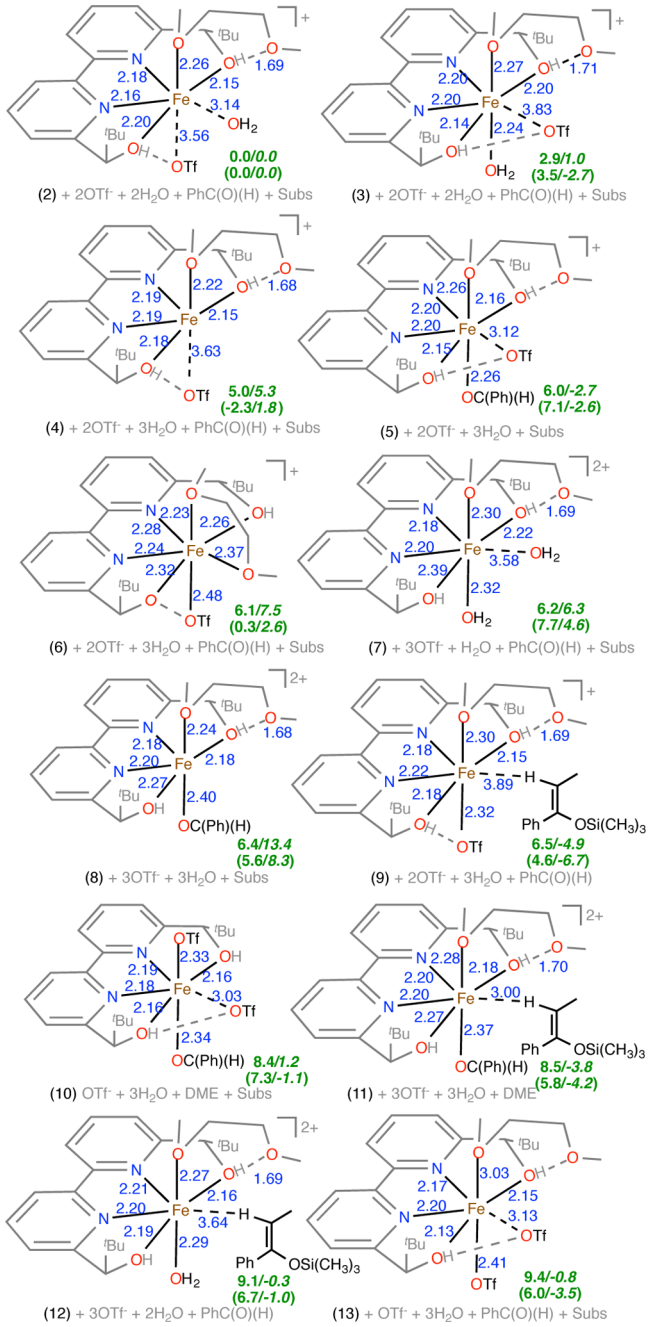

Figure 2. Low energy complexes in solution. All optimized structures are in the quintet state. Relative energies (green) are in kcal mol^{-1} (ΔG values are in plane text, ΔE values are in italics), M06L values are in parentheses, and bond lengths (blue) are in Å.

stability. (iii) Binding of silyl enol ether (Subs) on Fe(II) is not favorable. (iv) Total charge of the most stable complexes (**2**-**6**) is +1, implying that coordination of two (or more) OTf$^-$ ligands or two (or more) H$_2$O ligands is not favorable.

In order to get a better understanding of the factors that govern the stability of the possible complexes, we have performed a regression analysis. Here, we used relative energy (ΔE or ΔG) of the complexes as the dependent variable, while the number of ligands (n) in the metal coordination sphere was the independent variables (see Supporting Information for more details, page S4−S7). On the basis of our analysis, approximate ΔE and ΔG of the complexes can be written as

DOI: 10.1021/jacs.5b05835
J. Am. Chem. Soc. 2015, 137, 11085−11094

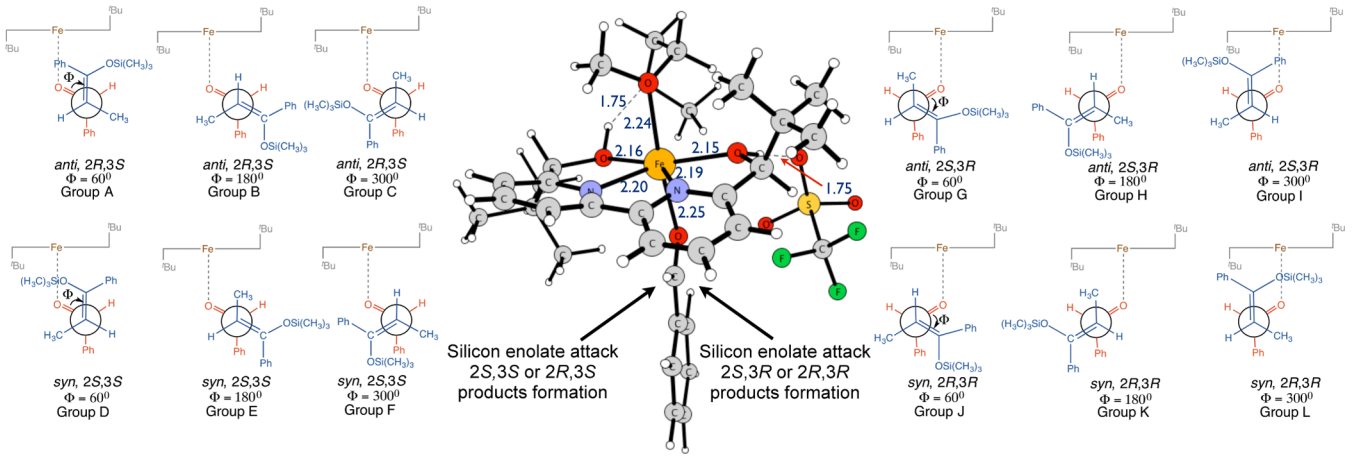

Figure 3. Possible transition state conformations associated with the carbon−carbon bond formation starting from 5.

$$\Delta E = -12.44n(\mathrm{OTf}^-) - 6.68n(\mathrm{H_2O}) - 10.37n(\mathrm{PhCOH}) - 18.58n(\mathrm{DME}) - 14.27n(\mathrm{Subs}) + 39.69 \quad (1)$$

$$\Delta G = -3.15n(\mathrm{OTf} -) - 0.28n(\mathrm{H_2O}) - 1.41n(\mathrm{PhCOH}) - 10.99n(\mathrm{DME}) - 0.07n(\mathrm{Subs}) + 20.57 \quad (2)$$

The coefficients of the eq 1 provide the approximate potential energy contributions for the total energy of the individual ligand upon coordination to Fe(II). The energetic preference would follow the order of DME > Subs > OTf > PhCOH > H_2O. In eq 2, both entropic and potential contributions are taken into account, and therefore coordination preference of the ligands can be determined from the coefficients in this equation. The coordination preference followes the order of DME > OTf^- > H_2O > PhCOH > Subs. The ΔG results suggested that the most favorable ligands are one DME and one OTf^-. Therefore, these two ligands can be found in the most stable complexes (**2**–**9**), and filled two vacant coordination sites. Even though bulky silyl enol ether provides a significant potential energy contribution, its large entropic contribution lowers the coordination preference.

Following the above general rules, complex **2**, a seven-coordinate complex coordinated by L1, DME, OTf^-, and H_2O is the thermodynamically most stable species. We use **2** as the origin for reporting relative energies. Its isomeric form, **3**, is only 2.9 kcal mol^{-1} higher, and therefore both **2** and **3** may be possible in the solution. Complex **4**, a six-coordinate complex, has L1, DME, and OTf^- ligands in its metal coordination sphere, and this complex is only 5.0 kcal mol^{-1} higher than the most stable complex, **2**. Interestingly, $[(L1)Fe(II)\ (OTf)\ (DME)]^+$ complex (i.e., **4** or its seven-coordinate isomeric form **6**) was detected by the ESI-MS studies.[46] Complex **5** holds L1, DME, PhC(O)(H) and OTf^- ligands, and this complex is 6.0 kcal mol^{-1} higher than **2**. In **5**, benzaldyhyde is coordinated at the axial position and an OTf^- ligand is weakly bound to the hydroxyl group of L1 through hydrogen-bonding, which is important for the stability of the complex. For instance, in the absence of the dangling OTf^- ligand, resulting six-coordinate complex, **8**, is 0.4 kcal mol^{-1} higher than **5**. Despite several attempts, we were unable to coordinate the benzaldehyde ligand from the equatorial direction due to strong *trans* effect from L1. Both **5** and **8** hold a benzaldehyde at the metal coordination sphere, and therefore both complexes may contribute to the carbon−carbon bond formation. Among the other low-energy complexes in solution, **10** and **11** structures also have a benzaldehyde ligand at the axial position. These complexes are however relatively higher in energy, and therefore their contribution to the overall rate of the carbon−carbon bond formation would be small, if other lower energy species are reactive. It is important to note that the silyl enol ether binding on the metal center via its unsaturated C = C bond is not favored due to steric repulsions. As a result, carbon−carbon bond formation would not occur as an inner-sphere fashion. However, silyl enol ether binds weakly, and the resulting complex, **11**, is 2.5 kcal mol^{-1} higher than **5**.

On the basis of the above analysis, we conclude that the thermodynamically most stable complex in solution is **2**. Complexes **5**, **8**, **10**, and **11**, all having the reacting benzaldehyde at an axial position, can be the active intermediates for the carbon−carbon formation. Starting from the most stable complex **2**, the active intermediates can be formed through ligand exchange process. Search for TSs for the conversion of **2** to **5**, **5** to **8**, **5** to **10**, and **8** to **11** via an associated mechanism did not provide any TS. The energy required for this ligand exchange process will be at most several kcal mol^{-1}, and should take place easily under the experimental conditions. When we have used the M06L functional, some minor changes were observed for the thermodynamic stability of the possible complexes. For instance, M06L suggested that the most stable complex is **4**. However, **2** is only 2.3 kcal mol^{-1} higher in energy. According to M06L ΔG values, most stable active intermediate is **8**, while **5** is only 1.5 kcal mol^{-1} higher in energy. These minor changes do not play a major role on the overall mechanism (vide infra).

Starting from the lowest energy *active* intermediates **5**, silyl enol can attack from either of the two directions, leading to the carbon−carbon bond formation. Structural difference between **5** and **8** is that the latter species has no OTf^- ligand at the equatorial position, and the energy difference of **5** and **8** is only 0.4 kcal mol^{-1}. Therefore, at first we have performed a systematic search to identify the low energy transition states for carbon−carbon bond formation starting from **5**. Then, the lowest energy transition states leading to (2*S*,3*S*), (2*R*,3*R*), (2*S*,3*R*), and (2*R*,3*S*) forms of the products were identified, and the analogs transition states that originate from **8** were searched. Transition states come from **10** and **11** were not taken into account in the discussion due to the following reasons; (a) In **8**, equatorial position is vacant (i.e., silyl enol ether substrate is at the infinity), while **11** has a silyl enol ether

DOI: 10.1021/jacs.5b05835
J. Am. Chem. Soc. 2015, 137, 11085−11094

substrate weakly coordinated at this position. As a result, the transition states that originate from **11** are equivalent to those from **8**. (b) Both **5** and **10** complexes differ only from the axial ligand of the upper part, where the former system has a DME ligand, while latter system hold an OTf^- ligand. As the carbon−carbon bond formation occurs at the bottom part of the complexes, both **5** and **10** would give similar steric repulsions for the carbon−carbon bond formation. At the same time, it is important to note that **10** is 2.4 kcal mol^{-1} higher than **5**. As a result, transition states that originate from **10** would be higher than that from **5.**

As discussed in the preceding paragraph, the bulky silyl enol ether cannot coordinate to the metal center through its C = C bond. *Therefore, the reaction between silyl enol ether and the active intermediates has to take place through an outer-sphere process.* With a detailed description of an active species in hand, our next step is to discuss the details of the carbon−carbon bond formation step.

3. Enantio- and Diastereoselectivity at the Carbon−Carbon Bond Formation Step. Our next step is to elucidate the origin of the enantioselectivity and diastereoselectivity, where we focus on the selectivity-determining carbon−carbon bond formation step, starting from the active species **5**. Enantioselectivity and diastereoselectivity of the reaction are determined by the approach direction and relative orientation of silyl enol ether. On the basis of the stereoisomers of the resultant product, the transition states can be categorized into four groups, (2*S*,3*S*), (2*R*,3*R*), (2*S*,3*R*), and (2*R*,3*S*), as shown in Figure 3. For each group, there should be several subgroups whose dihedral angles (Φ) around the reactive carbon−carbon bonds are different. We have performed MC-AFIR search to sample all possible lower energy conformations of various approximate transition states for the carbon−carbon bond formation starting from the most stable active intermediate **5** in solution.

Starting from **5**, the randomly selected initial structures with different orientations and approach directions of the silyl enol ether, AFIR optimizations gave rise to 41 approximate transition states (Figure S2). On the basis of the O—(Ph)-(H)C—C═C dihedral angles and orientation of the silyl enol ether, TSs can be categorized into 12 different groups (Figure 3). Among them, the lowest energy TSs (within 20 kcal mol^{-1}) were fully optimized, where we have found 15 TSs (Figure 4, Table 1). No transition states were found for groups A, D, I and L due to steric repulsions between the bulky groups of L1 and

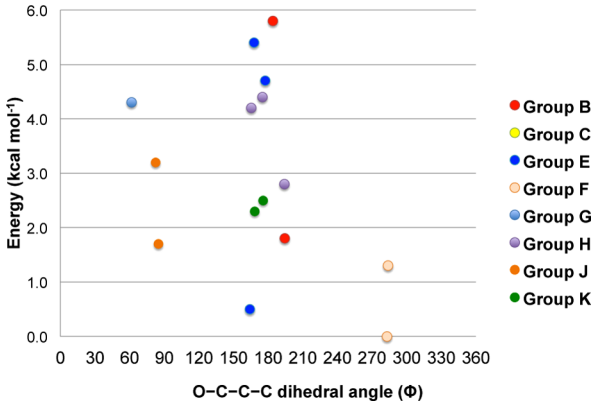

Figure 4. Relative energy (ΔΔ*G*) and dihedral angle (Φ) (in deg) of the optimized TSs. The energy is relative to TS1.

silyl enol ether. Among the fully optimized transition states (Table 1), **TS1** (Group F) is the lowest energy transition state, giving rise to the desired stereo product, 2*S*,3*S* (*syn*), which is in agreement with the experimental results. This transition state is 24.6 kcal mol^{-1} higher than the thermodynamically most stable complex **2**. The same product can be obtained through **TS2** (Group E) and **TS3** (Group F), which are only 0.5 and 1.3 kcal mol^{-1} higher than **TS1**, respectively. Among the competing paths, **TS4** (26.3 kcal mol^{-1}, Group J) leads to 2*R*,3*R* (*syn*) form of the product. The 2*R*,3*S* (*anti*) form of the product comes from **TS5** (26.4 kcal mol^{-1}, Group B), while 2*S*,3*R* (*anti*) product derives from **TS6** (26.9 kcal mol^{-1}, Group H).

Next, the barrier for the carbon−carbon bond formation was calculated starting from the slightly high-energy active intermediate, **8**. Most striking difference in **8** is the absence of the dangling OTf^-. For this purpose, only the key transition states leading to (2*S*,3*S*), (2*R*,3*R*), (2*R*,3*S*), and (2*S*,3*R*) products were taken into account, and the calculated barriers were 25.1 (**TS1′**, Group F), 28.5 (**TS2′**, Group J), 31.1 (**TS3′**, Group B), and 28.8 (**TS4′**, Group H) kcal mol^{-1}, respectively. Among these transition states, only **TS1′** is a minor contributor to the overall rate of the (2*S*,3*S*) product formation, whereas the remaining three transition states too high in energy to contribute to the reaction. Then, we have used the M06L functional to calculate the key transition states leading to (2*S*,3*S*) and (2*R*,3*R*) products. The major product, (2*S*,3*S*), comes from **TS1** (21.4 kcal mol^{-1}) and **TS1′** (21.8 kcal mol^{-1}), while **TS4** (23.2 kcal mol^{-1}) leads to the minor (2*R*,3*R*) product. Relative energies between **TS1** and **TS1′** (0.4 kcal mol^{-1}) and **TS1** and **TS4** (1.8 kcal mol^{-1}) are in agreement with the B3LYP-D3 results. Also, B3LYP-D3 results reproduced the experimental enantiomeric excess and *syn:anti* ratio (vide infra). Therefore, we did not calculate all possible transition states with the M06 functional.

On the basis of the computed transition states (B3LYP-D3), calculated enantiomeric excess of 95% (*syn*) with ΔΔ*G* and 86% with ΔΔ*E* is in agreement with the experimental results (75%). It is important to note that we have calculated Gibbs free by considering translational, rotational, and vibrational contributions.[90,92,110−112] On the basis of the transition states leading to *syn* and *anti* products, calculated *syn:anti* ratio of 98:2 with ΔΔ*G* and 99:1 with ΔΔ*E* is also in agreement with the experimental ratio of 97:3. The energetically lowest optimized structures, **TS1** giving 2*S*,3*S* (*syn*) product and **TS4** giving 2*R*,3*R* (*syn*), are the major contributors for the enantiomeric excess (Figure 5). Gibbs free energy of **TS4** relative to **TS1** is +1.7 kcal mol^{-1}, and this can be decomposed into electronic energy contribution of +1.2 kcal mol^{-1} and entropic effect of +0.5 kcal mol^{-1}. It is important to note that the carbon−carbon bond distance in **TS4** is 1.86 Å, which is 0.02 Å shorter than in **TS1** (Figure 5). With a tighter TS structure, less favorable entropic contribution can be expected for **TS4**.

We have performed an EDA for ΔΔ*E* = +1.2 kcal mol^{-1} between **TS4** and **TS1** (Table 2). According to the EDA, this energy difference is controlled by ΔDEF (+2.2 kcal mol^{-1}), where contributions from the catalyst (A), benzaldehyde (B), and silyl enol ether (C) are −0.3, + 1.2, and +1.3 kcal mol^{-1}, respectively. One can say that the aldehyde and silyl enol ether have to be distorted more to reach **TS4** than to **TS1** during carbon−carbon bond formation. At the same time, EDA shows negative contributions for ΔINT, ΔINT_{AB} (−0.5 kcal mol^{-1}) and $\Delta INT_{(AB)C}$ (−0.5 kcal mol^{-1}), implying better interactions at **TS4**. During the carbon−carbon bond formation,

DOI: 10.1021/jacs.5b05835
J. Am. Chem. Soc. 2015, 137, 11085−11094

Table 1. Transition States for the Carbon−Carbon Bond Formation Starting from Two Active Species 5 and 8, Their Key Structural Parameters, Relative Energies and Existence Probability[a]

TSs (active species 5)	group	Φ (deg)	r(C−C) (Å)	product		ΔG (kcal mol^{-1})	ΔΔG (ΔΔE) (kcal mol^{-1})	existence probability (%)
TS1	F	283.0	1.87	2*S*,3*S*	*syn*	24.6	0.0 (0.0)	55.7 (67.7)
TS2	E	164.1	1.88	2*S*,3*S*	*syn*	25.1	0.5 (0.7)	22.2 (17.2)
TS3	F	283.3	1.84	2*S*,3*S*	*syn*	25.9	1.3 (1.0)	5.1 (4.0)
TS4	J	85.0	1.86	2*R*,3*R*	*syn*	26.3	1.7 (1.2)	2.4 (7.3)
TS5	B	194.4	1.85	2*R*,3*S*	*anti*	26.4	1.8 (3.1)	2.0 (0.2)
TS6	H	168.5	1.88	2*S*,3*R*	*anti*	26.9	2.3 (3.3)	0.8 (0.1)
TS7	E	175.7	1.92	2*S*,3*S*	*syn*	27.1	2.5 (2.4)	0.6 (0.9)
TS8	H	194.0	1.85	2*S*,3*R*	*anti*	27.4	2.8 (2.2)	0.3 (1.3)
TS9	F	82.5	1.85	2*S*,3*S*	*syn*	27.8	3.2 (2.3)	0.2 (1.1)
TS10	K	165.5	1.86	2*R*,3*R*	*syn*	28.8	4.2 (3.6)	0.0 (0.0)
TS11	G	61.6	1.85	2*S*,3*R*	*anti*	28.9	4.3 (4.3)	0.0 (0.1)
TS12	E	175.9	1.85	2*S*,3*S*	*syn*	29.0	4.4 (3.4)	0.0 (0.0)
TS13	E	177.6	1.89	2*S*,3*S*	*syn*	29.3	4.7 (4.5)	0.0 (0.0)
TS14	K	167.7	1.88	2*R*,3*R*	*syn*	30.0	5.4 (6.9)	0.0 (0.0)
TS15	B	184.0	1.88	2*R*,3*S*	*anti*	30.4	5.8 (6.2)	0.0 (0.0)
TSs (active species 8)								
TS1′ + OTf$^-$	F	282.1	1.86	2*S*,3*S*	*syn*	25.5	0.9 (14.2)	10.6 (0.0)
TS2′ + OTf$^-$	J	78.5	1.86	2*R*,3*R*	*syn*	28.5	3.9 (16.0)	0.0 (0.0)
TS3′ + OTf$^-$	B	178.6	1.90	2*R*,3*S*	*anti*	31.1	6.5 (20.5)	0.0 (0.0)
TS4′ + OTf$^-$	H	190.9	1.94	2*S*,3*R*	*anti*	28.8	4.3 (17.6)	0.0 (0.0)

[a]The values in parentheses derive from Δ*E*.

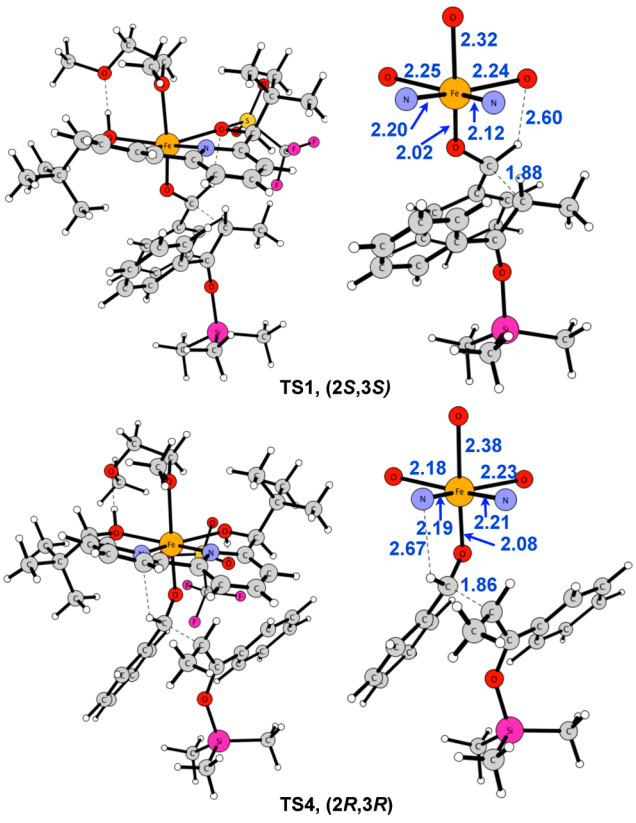

Figure 5. Optimized structures of **TS1** and **TS4**.

benzaldehyde unit undergoes clock-wise (**TS4**) or anticlock-wise (**TS1**) rotations. In the resulting TSs, hydrogen bonding occurs between the hydrogen atom of the aldehyde and nitrogen atom of L1 in **TS4**, and between the hydrogen atom of the aldehyde and oxygen atom of L1 in **TS1**. According to ΔINT_{AB} = −0.5 kcal mol^{-1}, the former scenario is more favorable. In **TS4**, silyl enol ether is closer to the catalyst than in **TS1**, resulting in the stronger interaction between catalyst/benzaldehyde (A+B) and silyl enol ether (C) with $\Delta INT_{(AB)C}$ = −0.5 kcal mol^{-1}.

Table 2. EDA for the Potential Energy Difference (ΔΔ*E*) between the Key Transition States, TS1 and TS4[a]

	DEF (DEF$_A$, DEF$_B$, DEF$_C$)	INT$_{AB}$	INT$_{(AB)C}$	Δ*E*
TS1	47.8 (10.3, 23.1, 14.4)	−14.5	−42.4	−9.0
TS4	50.0 (10.0, 24.3, 15.7)	−15.0	−42.8	−7.8
	ΔDEF	ΔINT$_{AB}$	ΔINT$_{(AB)C}$	ΔΔ*E*
	+2.2 (−0.3, +1.2, +1.3)	−0.5	−0.5	+1.2

[a]Energies are in kcal mol^{-1}.

In terms of improving the catalytic system to obtain better enantiomeric excess (more positive ΔΔ*E*), two factors can be considered. (1) More positive ΔDEF; this may be done by using bulky substituents in the silyl enol ether. (2) Less negative or more positive ΔINT; this may be achieved by modifying the tetra dentate ligand, L1. For instance, ΔINT_{AB} can be vanished if the all donor atoms of L1 are oxygen (or all are nitrogen).

Full Catalytic Cycle. Now we are in the position to discuss the full catalytic cycle for the reaction. Calculated free energy profile for the overall reaction is shown in Figure 6. The reaction starts from the thermodynamically most stable complex **2**. Then, weakly bound H_2O ligand in the equatorial position dissociates, giving rise to **4** (+5.0 kcal mol^{-1}). After that, benzaldehyde coordination on **4** leads to the active intermediate **5**, which is 6.0 kcal mol^{-1} higher than **2**. As the next step, the selectivity determining carbon−carbon bond formation occurs with the overall barrier of 24.6 kcal mol^{-1}, leading to the desired 2*S*,3*S* (*syn*) form of the product. The resulting species, **I1**, is 21.6 kcal mol^{-1} above the entry point of the free energy profile. Starting from **I1**, binding a water molecule on the oxygen atom of benzaldehyde is possible, and the resulting species, **I2**, is only 2.5 kcal mol^{-1} higher than **I1**. Then, a proton transfer takes place through TS_H (28.0 kcal

DOI: 10.1021/jacs.5b05835
J. Am. Chem. Soc. 2015, 137, 11085−11094

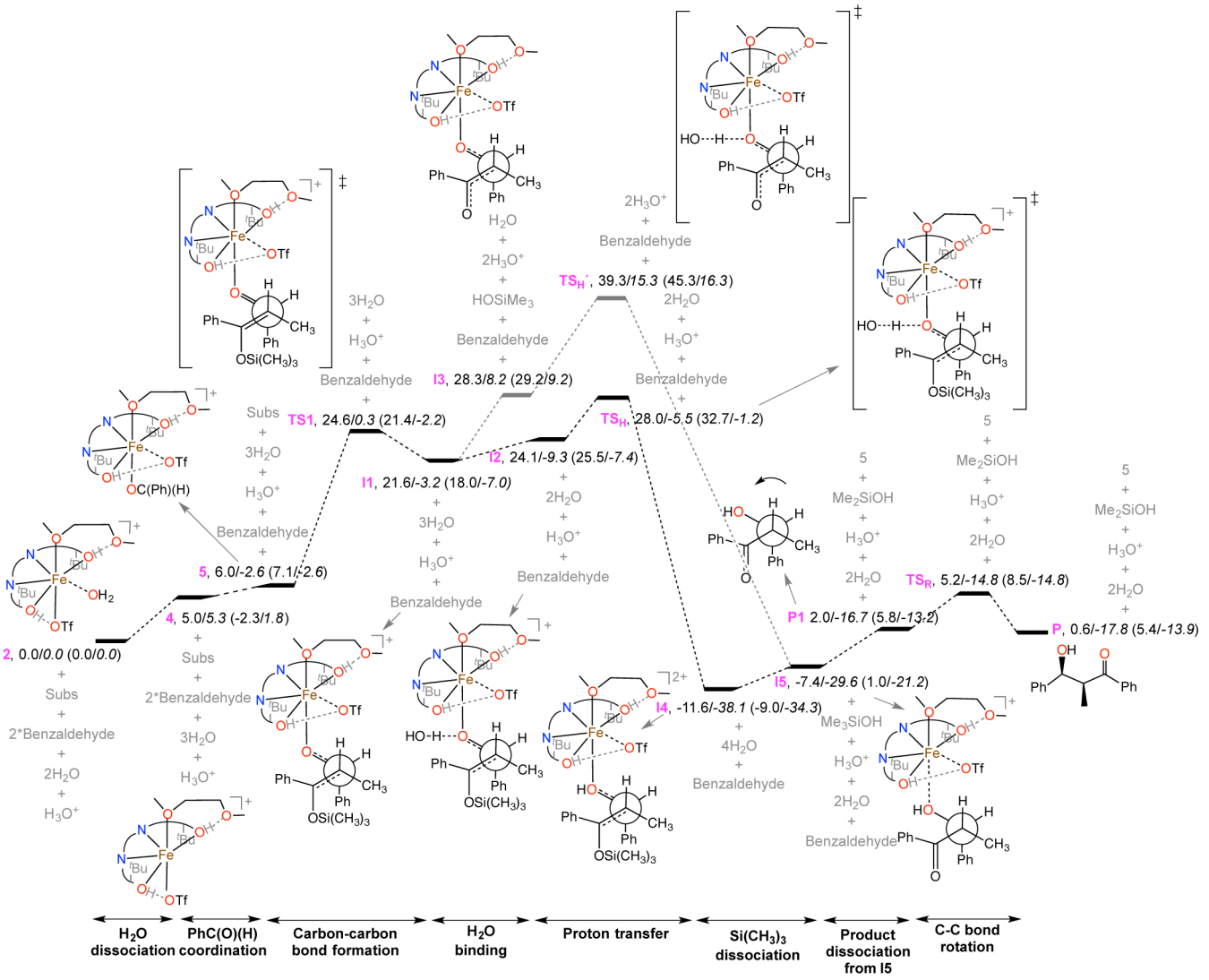

Figure 6. Free energy profile (kcal mol^{-1}) for the Mukaiyama aldol reaction of silicon enolates with aldehydes catalyzed by a chiral Fe(II) complexes in aqueous media (ΔG values are in plane text, ΔE values are in italics, and M06L values are in parentheses).

mol^{-1}), resulting an intermediate **I4** (−11.6 kcal mol^{-1}). **TS$_H$** is the highest point of the free energy profile, and therefore the rate-limiting step. Starting from **I1**, dissociation of the − $SiMe_3$ group is rather unlikely, as this process is endothermic by 6.6 kcal mol^{-1}, and the subsequent transition state for the proton transfer process (TS$_H$´) is further 11.0 kcal mol^{-1} higher in energy. Starting from **I4**, the next step of the mechanism is the dissociation of -$SiMe_3$ group that leads to **I5**, and this species is 4.2 kcal mol^{-1} higher than **I4**. After that, product (**P1**) is removed from the metal coordination sphere, and a benzaldehyde ligand is coordinated to yield the active species **5**, which is ready for the next catalytic cycle. More stable isomer of the product, **P**, can be formed through rotation of the carbon−carbon bond (**TS$_R$**), and this step requires only 3.2 kcal mol^{-1}.

When we used the M06L functional, overall mechanism remains unchanged. Both B3LYP-D3 and M06L functionals suggested that the rate-determining step is the proton transfer between H_2O and the carbonyl group of aldehyde (**TS$_H$**), while the carbon−carbon bond formation (**TS1**) is the selectivity-determining step. Energy separation between **TS$_H$** and **TS1** is +3.4 kcal mol^{-1} for B3LYP-D3 and +11.3 kcal mol^{-1} for M06L. Similar picture can be observed with the BP86-D3 (+3.7 kcal mol^{-1}) and B97D3 (+10.7 kcal mol^{-1}) functionals. According to these results, proton transfer between H_2O (**TS$_H$**) and the carbonyl group is the rate-determining step in all cases.

CONCLUSIONS

We have rationalized the mechanism of Mukaiyama aldol reactions of silyl enol ethers with aldehydes catalyzed by chiral Fe(II) complexes in aqueous media. Our survey on the electronic structure of the seven- or six-coordinate Fe(II) complexes suggested that the high-spin quintet state is thermodynamically stable, while the triplet or the singlet states are significantly higher in energy. Therefore, the overall mechanism operates on the quintet state. Several complexes are possible in the solution. Of these, seven-coordinate [(L1)Fe(II) (OTf) (DME)(H_2O)]$^+$ complex (**2**) is the thermodynamically most stable complex, and [(L1)Fe(II) (OTf) (DME) (PhC(O)H)]$^+$ (**5**) is the most stable *active* species for the carbon−carbon bond formation. In **5**, a dangling OTf^- ligand is found, which is attached to the −OH group of L1 via hydrogen binding. This feature helps to stabilize **5** in solution and lower the barrier for the carbon−carbon bond

DOI: 10.1021/jacs.5b05835
J. Am. Chem. Soc. 2015, 137, 11085−11094

formation. The carbon−carbon bond formation is the selectivity-determining step of the reaction, while the proton transfer between solvent (H_2O) and of the carbonyl group of aldehyde is the rate-determining step. The remaining steps of the mechanism are relatively straightforward. These MC-AFIR results identified important competing reaction pathways for the selectivity-determining carbon−carbon bond formation. Calculated enantioselectivity and diastereoselectivity are in good agreement with the experimental results. Overall, the proposed mechanism is consistent with the experiments. This study will guide the design of transition metal catalysts for Mukaiyama aldol reactions in aqueous media.

■ ASSOCIATED CONTENT

Supporting Information

The Supporting Information is available free of charge on the ACS Publications website at DOI: 10.1021/jacs.5b05835.

Possible spin states of $[(L1)Fe(II)DME(H_2O)]^{2+}$ (**1**), $[(L1)Fe(II)\ (DME)(H_2O)\ (OTf)]^{+}$ (**2**), $[(L1)Fe(II)\ (DME)\ (OTf)]^{+}$ (**4**), and $[(L1)Fe(II)\ (DME)\ (PhC(O)H)\ (OTf)]^{+}$ (**5**) complexes. Possible structures in solution and their energies. Regression analysis. Approximate transition states from MC-AFIR search. Energies of the optimized structures. Cartesian coordinates of the optimized structures. (PDF)

■ AUTHOR INFORMATION

Corresponding Author

*morokuma@fukui.kyoto-u.ac.jp

Notes

The authors declare no competing financial interest.

■ ACKNOWLEDGMENTS

The authors are grateful to Prof. Satoshi Maeda of Hokkaido University for the developmental version of the GRRM code. WMCS acknowledge to the Japan Society for the Promotion of Science (JSPS, No: P14334) for a Foreign Postdoctoral Fellowship. MH acknowledges the Fukui Fellowship of Kyoto University and Collaborative Research Program for Young Scientists of ACCMS and IIMC, Kyoto University. This work was partly supported by Grants-in-Aid from MEXT for Innovative Areas (Soft Molecular Systems, No. 26104519), for Young Scientist (B) (No. 26810005) to MH and for Scientific Research (No. 25109525, 15H00938 and 15H02158) to KM at Kyoto University. The Computer resources at the Institute for Information Management and Communication (IIMC) at Kyoto University and Research Center of Computational Science (RCCS) at the Institute for Molecular Science are also acknowledged.

■ REFERENCES

(1) Miyaura, N.; Suzuki, A. *Chem. Rev.* **1995**, *95*, 2457.
(2) Martin, R.; Buchwald, S. L. *Acc. Chem. Res.* **2008**, *41*, 1461.
(3) Beletskaya, I. P.; Cheprakov, A. V. *Chem. Rev.* **2000**, *100*, 3009.
(4) Mc Cartney, D.; Guiry, P. J. *Chem. Soc. Rev.* **2011**, *40*, 5122.
(5) Cabri, W.; Candiani, I. *Acc. Chem. Res.* **1995**, *28*, 2.
(6) Guiry, P. J.; Hennessy, A. J.; Cahill, J. P. *Top. Catal.* **1997**, *4*, 311.
(7) Maryanoff, B. E.; Reitz, A. B. *Chem. Rev.* **1989**, *89*, 863.
(8) Byrne, P. A.; Gilheany, D. G. *Chem. Soc. Rev.* **2013**, *42*, 6670.
(9) Vougioukalakis, G. C.; Grubbs, R. H. *Chem. Rev.* **2010**, *110*, 1746.
(10) Grubbs, R. H.; Chang, S. *Tetrahedron* **1998**, *54*, 4413.
(11) Grubbs, R. H. *Tetrahedron* **2004**, *60*, 7117.
(12) Hoveyda, A. H.; Zhugralin, A. R. *Nature* **2007**, *450*, 243.
(13) Kress, S.; Blechert, S. *Chem. Soc. Rev.* **2012**, *41*, 4389.
(14) Baratta, W.; DelZotto, A.; Rigo, P. *Chem. Commun.* **1997**, 2163.
(15) Hodgson, D. M.; Angrish, D. *Chem. Commun.* **2005**, 4902.
(16) Bray, C. V. L; Derien, S.; Dixneuf, P. H. *Angew. Chem., Int. Ed.* **2009**, *48*, 1439.
(17) Hansen, J. H.; Parr, B. T.; Pelphrey, P.; Jin, Q. H.; Autschbach, J.; Davies, H. M. L. *Angew. Chem., Int. Ed.* **2011**, *50*, 2544.
(18) Rivilla, I.; Sameera, W. M. C.; Alvarez, E.; Diaz-Requejo, M. M.; Maseras, F.; Perez, P. J. *Dalton T* **2013**, *42*, 4132.
(19) Palomo, C.; Oiarbide, M.; Garcia, J. M. *Chem. - Eur. J.* **2002**, *8*, 37.
(20) Palomo, C.; Oiarbide, M.; Garcia, J. M. *Chem. Soc. Rev.* **2004**, *33*, 65.
(21) Schetter, B.; Mahrwald, R. *Angew. Chem., Int. Ed.* **2006**, *45*, 7506.
(22) Trost, B. M.; Brindle, C. S. *Chem. Soc. Rev.* **2010**, *39*, 1600.
(23) Mukaiyama, T.; Narasaka, K.; Banno, K. *Chem. Lett.* **1973**, 1011.
(24) Mukaiyama, T.; Izawa, T.; Saigo, K. *Chem. Lett.* **1974**, 323.
(25) Mukaiyama, T.; Banno, K.; Narasaka, K. *J. Am. Chem. Soc.* **1974**, *96*, 7503.
(26) Mukaiyama, T. *Angew. Chem., Int. Ed.* **2004**, *43*, 5590.
(27) Matsuo, J.; Murakami, M. *Angew. Chem., Int. Ed.* **2013**, *52*, 9109.
(28) Kan, S. B. J.; Ng, K. K. H.; Paterson, I. *Angew. Chem., Int. Ed.* **2013**, *52*, 9097.
(29) Kobayashi, S. *Synlett* **1994**, *1994*, 689.
(30) Kobayashi, S.; Hachiya, I. *J. Org. Chem.* **1994**, *59*, 3590.
(31) Kobayashi, S.; Sugiura, M.; Kitagawa, H.; Lam, W. W. L. *Chem. Rev.* **2002**, *102*, 2227.
(32) Kitanosono, T.; Kobayashi, S. *Adv. Synth. Catal.* **2013**, *355*, 3095.
(33) Kobayashi, S.; Nagayama, S.; Busujima, T. *J. Am. Chem. Soc.* **1998**, *120*, 8287.
(34) Kitanosono, T.; Kobayashi, S. *Chem. Rec* **2014**, *14*, 130.
(35) Nagayama, S.; Kobayashi, S. *J. Am. Chem. Soc.* **2000**, *122*, 11531.
(36) Hamada, T.; Manabe, K.; Kobayashi, S. *Yuki Gosei Kagaku Kyokaishi* **2003**, *61*, 445.
(37) Hamada, T.; Manabe, K.; Ishikawa, S.; Nagayama, S.; Shiro, M.; Kobayashi, S. *J. Am. Chem. Soc.* **2003**, *125*, 2989.
(38) Li, H. J.; Tian, H. Y.; Wu, Y. C.; Chen, Y. J.; Liu, L.; Wang, D.; Li, C. J. *Adv. Synth. Catal.* **2005**, *347*, 1247.
(39) Jankowska, J.; Mlynarski, J. *J. Org. Chem.* **2006**, *71*, 1317.
(40) Jankowska, J.; Paradowska, J.; Rakiel, B.; Mlynarski, J. *J. Org. Chem.* **2007**, *72*, 2228.
(41) Woyciechowska, M.; Forcher, G.; Buda, S.; Mlynarski, J. *Chem. Commun.* **2012**, *48*, 11029.
(42) Mei, Y. J.; Dissanayake, P.; Allen, M. J. *J. Am. Chem. Soc.* **2010**, *132*, 12871.
(43) Mei, Y. J.; Averill, D. J.; Allen, M. J. *J. Org. Chem.* **2012**, *77*, 5624.
(44) Bolm, C.; Zehnder, M.; Bur, D. *Angew. Chem., Int. Ed. Engl.* **1990**, *29*, 205.
(45) Ollevier, T.; Plancq, B. *Chem. Commun.* **2012**, *48*, 2289.
(46) Kitanosono, T.; Ollevier, T.; Kobayashi, S. *Chem. - Asian J.* **2013**, *8*, 3051.
(47) Ishikawa, S.; Hamada, T.; Manabe, K.; Kobayashi, S. *J. Am. Chem. Soc.* **2004**, *126*, 12236.
(48) Kobayashi, S.; Ogino, T.; Shimizu, H.; Ishikawa, S.; Hamada, T.; Manabe, K. *Org. Lett.* **2005**, *7*, 4729.
(49) Kokubo, M.; Ogawa, C.; Kobayashi, S. *Angew. Chem., Int. Ed.* **2008**, *47*, 6909.
(50) Kobayashi, S.; Kokubo, M.; Kawasumi, K.; Nagano, T. *Chem. - Asian J.* **2010**, *5*, 490.
(51) Azoulay, S.; Manabe, K.; Kobayashi, S. *Org. Lett.* **2005**, *7*, 4593.
(52) Nandakumar, M. V.; Tschop, A.; Krautscheid, H.; Schneider, C. *Chem. Commun.* **2007**, 2756.
(53) Kokubo, M.; Kobayashi, S. *Chem. - Asian J.* **2009**, *4*, 526.
(54) Gung, B. W.; Zhu, Z. H.; Fouch, R. A. *J. Org. Chem.* **1995**, *60*, 2860.
(55) Wong, C. T.; Wong, M. W. *J. Org. Chem.* **2005**, *70*, 124.

DOI: 10.1021/jacs.5b05835
J. Am. Chem. Soc. 2015, 137, 11085−11094

(56) Cheong, P. H. Y.; Legault, C. Y.; Um, J. M.; Celebi-Olcum, N.; Houk, K. N. *Chem. Rev.* **2011**, *111*, 5042.
(57) Allemann, C.; Um, J. M.; Houk, K. N. *J. Mol. Catal. A: Chem.* **2010**, *324*, 31.
(58) Duarte, F. J. S.; Cabrita, E. J.; Frenking, G.; Santos, G. *Eur. J. Org. Chem.* **2008**, *2008*, 3397.
(59) Denmark, S. E.; Fan, Y.; Eastgate, M. D. *J. Org. Chem.* **2005**, *70*, 5235.
(60) Branchadell, V.; Crevisy, C.; Gree, R. *Chem. - Eur. J.* **2004**, *10*, 5795.
(61) Clemente, F. R.; Houk, K. N. *Angew. Chem., Int. Ed.* **2004**, *43*, 5766.
(62) Ruiz, M.; Ojea, V.; Quintela, J. M. *Tetrahedron: Asymmetry* **2002**, *13*, 1863.
(63) Arno, M.; Domingo, L. R. *Theor. Chem. Acc.* **2002**, *108*, 232.
(64) Bahmanyar, S.; Houk, K. N. *Org. Lett.* **2003**, *5*, 1249.
(65) Bouillon, J. P.; Portella, C.; Bouquant, J.; Humbel, S. *J. Org. Chem.* **2000**, *65*, 5823.
(66) Bernardi, A.; Karamfilova, K.; Sanguinetti, S.; Scolastico, C. *Tetrahedron* **1997**, *53*, 13009.
(67) Wong, C. T.; Wong, M. W. *J. Org. Chem.* **2007**, *72*, 1425.
(68) Wang, L.; Wong, M. W. *Tetrahedron Lett.* **2008**, *49*, 3916.
(69) Lee, J. M.; Helquist, P.; Wiest, O. *J. Am. Chem. Soc.* **2012**, *134*, 14973.
(70) Maeda, S.; Morokuma, K. *J. Chem. Phys.* **2010**, *132*, 241102.
(71) Maeda, S.; Morokuma, K. *J. Chem. Theory Comput.* **2011**, *7*, 2335.
(72) Maeda, S.; Ohno, K.; Morokuma, K. *Phys. Chem. Chem. Phys.* **2013**, *15*, 3683.
(73) Hatanaka, M.; Morokuma, K. *J. Am. Chem. Soc.* **2013**, *135*, 13972.
(74) Hatanaka, M.; Maeda, S.; Morokuma, K. *J. Chem. Theory Comput.* **2013**, *9*, 2882.
(75) Becke, A. D. *Phys. Rev. A: At., Mol., Opt. Phys.* **1988**, *38*, 3098.
(76) Lee, C. T.; Yang, W. T.; Parr, R. G. *Phys. Rev. B: Condens. Matter Mater. Phys.* **1988**, *37*, 785.
(77) Miehlich, B.; Savin, A.; Stoll, H.; Preuss, H. *Chem. Phys. Lett.* **1989**, *157*, 200.
(78) Grimme, S.; Antony, J.; Ehrlich, S.; Krieg, H. *J. Chem. Phys.* **2010**, *132*, 154104.
(79) Frisch, M. J.; Trucks, G. W.; Schlegel, H. B.; Scuseria, G. E.; Robb, M. A.; Cheeseman, J. R.; Scalmani, G.; Barone, V.; Mennucci, B.; Petersson, G. A.; Nakatsuji, H.; Caricato, M.; Li, X.; Hratchian, H. P.; Izmaylov, A. F.; Bloino, J.; Zheng, G.; Sonnenberg, J. L.; Hada, M.; Ehara, M.; Toyota, K.; Fukuda, R.; Hasegawa, J.; Ishida, M.; Nakajima, T.; Honda, Y.; Kitao, O.; Nakai, H.; Vreven, T.; Montgomery, J. A., Jr.; Peralta, J. E.; Ogliaro, F.; Bearpark, M.; Heyd, J. J.; Brothers, E.; Kudin, K. N.; Staroverov, V. N.; Kobayashi, R.; Normand, J.; Raghavachari, K.; Rendell, A.; Burant, J. C.; Iyengar, S. S.; Tomasi, J.; Cossi, M.; Rega, N.; Millam, J. M.; Klene, M.; Knox, J. E.; Cross, J. B.; Bakken, V.; Adamo, C.; Jaramillo, J.; Gomperts, R.; Stratmann, R. E.; Yazyev, O.; Austin, A. J.; Cammi, R.; Pomelli, C.; Ochterski, J. W.; Martin, R. L.; Morokuma, K.; Zakrzewski, V. G.; Voth, G. A.; Salvador, P.; Dannenberg, J. J.; Dapprich, S.; Daniels, A. D.; Farkas, Ö.; Foresman, J. B.; Ortiz, J. V.; Cioslowski, J.; Fox, D. J. *Gaussian 09*, Revision D.01; Gaussian, Inc.: Wallingford, CT, 2009.
(80) Marenich, A. V.; Cramer, C. J.; Truhlar, D. G. *J. Phys. Chem. B* **2009**, *113*, 6378.
(81) Fuentealba, P.; Preuss, H.; Stoll, H.; Vonszentpaly, L. *Chem. Phys. Lett.* **1982**, *89*, 418.
(82) Dunning, T. H., Jr.; Hay, P. J. *Modern Theoretical Chemistry*; Plenum: New York, 1977; Vol. 3, pp 1−28.
(83) Ditchfie, R.; Hehre, W. J.; Pople, J. A. *J. Chem. Phys.* **1971**, *54*, 724.
(84) Hehre, W. J.; Ditchfie, R.; Pople, J. A. *J. Chem. Phys.* **1972**, *56*, 2257.
(85) Hariharan, P. C.; Pople, J. A. *Theor Chim Acta* **1973**, *28*, 213.
(86) Francl, M. M.; Pietro, W. J.; Hehre, W. J.; Binkley, J. S.; Gordon, M. S.; Defrees, D. J.; Pople, J. A. *J. Chem. Phys.* **1982**, *77*, 3654.
(87) Dunning, T. H. *J. Chem. Phys.* **1989**, *90*, 1007.
(88) Kendall, R. A.; Dunning, T. H.; Harrison, R. J. *J. Chem. Phys.* **1992**, *96*, 6796.
(89) Woon, D. E.; Dunning, T. H. *J. Chem. Phys.* **1993**, *98*, 1358.
(90) Tanaka, R.; Yamashita, M.; Chung, L. W.; Morokuma, K.; Nozaki, K. *Organometallics* **2011**, *30*, 6742.
(91) Strajbl, M.; Sham, Y. Y.; Villa, J.; Chu, Z. T.; Warshel, A. *J. Phys. Chem. B* **2000**, *104*, 4578.
(92) Hermans, J.; Wang, L. *J. Am. Chem. Soc.* **1997**, *119*, 2707.
(93) Yu, Z. X.; Caramella, P.; Houk, K. N. *J. Am. Chem. Soc.* **2003**, *125*, 15420.
(94) Harvey, J. N. *Faraday Discuss.* **2010**, *145*, 487.
(95) Ribeiro, A. J. M.; Ramos, M. J.; Fernandes, P. A. *J. Chem. Theory Comput.* **2010**, *6*, 2281.
(96) Ribeiro, R. F.; Marenich, A. V.; Cramer, C. J.; Truhlar, D. G. *J. Phys. Chem. B* **2011**, *115*, 14556.
(97) Maeda, S. H. Y.; Osada, Y.; Taketsugu, T.; Morokuma, K.; Ohno, K. *J. Am. Chem. Soc.* **2014**, *137*, 3433.
(98) Dapprich, S.; Komaromi, I.; Byun, K. S.; Morokuma, K.; Frisch, M. J. *J. Mol. Struct.: THEOCHEM* **1999**, *461*, 1.
(99) Vreven, T.; Byun, K. S.; Komaromi, I.; Dapprich, S.; Montgomery, J. A.; Morokuma, K.; Frisch, M. J. *J. Chem. Theory Comput.* **2006**, *2*, 815.
(100) Vreven, T.; Morokuma, K. *J. Comput. Chem.* **2000**, *21*, 1419.
(101) Maseras, F.; Morokuma, K. *J. Comput. Chem.* **1995**, *16*, 1170.
(102) Matsubara, T.; Sieber, S.; Morokuma, K. *Int. J. Quantum Chem.* **1996**, *60*, 1101.
(103) Svensson, M.; Humbel, S.; Froese, R. D. J.; Matsubara, T.; Sieber, S.; Morokuma, K. *J. Phys. Chem.* **1996**, *100*, 19357.
(104) Hay, P. J.; Wadt, W. R. *J. Chem. Phys.* **1985**, *82*, 270.
(105) Wadt, W. R.; Hay, P. J. *J. Chem. Phys.* **1985**, *82*, 284.
(106) Hay, P. J.; Wadt, W. R. *J. Chem. Phys.* **1985**, *82*, 299.
(107) Morokuma, K. *J. Chem. Phys.* **1971**, *55*, 1236.
(108) Kitaura, K.; Morokuma, K. *Int. J. Quantum Chem.* **1976**, *10*, 325.
(109) Hoffmann, R.; Beier, B. F.; Muetterties, E. L.; Rossi, A. R. *Inorg. Chem.* **1977**, *16*, 511.
(110) Yu, Z. X.; Houk, K. N. *J. Am. Chem. Soc.* **2003**, *125*, 13825.
(111) Sugiyama, A.; Ohnishi, Y. Y.; Nakaoka, M.; Nakao, Y.; Sato, H.; Sakaki, S.; Nakao, Y.; Hiyama, T. *J. Am. Chem. Soc.* **2008**, *130*, 12975.
(112) Ohnishi, Y.; Nakao, Y.; Sato, H.; Nakao, Y.; Hiyama, T.; Sakaki, S. *Organometallics* **2009**, *28*, 2583.

DOI: 10.1021/jacs.5b05835
J. Am. Chem. Soc. 2015, 137, 11085−11094